Detailed Numerical Investigation of a dc Sputter Magnetron

Ivan Kolev and Annemie Bogaerts

***Abstract*—A self-consistent 2d3v numerical model based on the Particle-in-cell/Monte Carlo collisions technique is developed to study the processes in dc sputter magnetrons. The model includes also modules for the transport of the sputtered atoms and the gas heating. The main discharge characteristics such as the electrical potential, the density distributions of all plasma species, the gas temperature distribution and the erosion profile are presented and compared to experimental data, whenever available.**

***Index Terms*—gas heating, magnetron, modeling, particle-in-cell (PIC), sputtering.**

I. Introduction

MAGNETRONS have been in use for sputtering and deposition of metal and nonmetal coatings since early 1970s. Different geometrical configurations (cylindrical, planar) and power supplies (dc, rf, pulsed) exist. A number of basic reviews and discussions of the topic are available [1]-[5]. One of the most used types of magnetrons is the planar magnetron with either a cylindrical or a rectangular cathode. In the circular version, a magnet is located behind the cathode (target). This magnet creates a magnetic field that is primarily parallel to the cathode surface between the magnetic poles. In this way, a strong magnetic trap for the electrons is created, allowing the discharge to be operated at low pressures (a few mtorr), with applied voltage much lower than required by the Paschen theory for a fixed pressure. Normally, when the circular configuration is used the magnetic field is axisymmetrical, with a strongly inhomogeneous spatial distribution. The magnetic strength in front of the cathode varies, typically, from 0.01 to 0.15 T. The presence of such field makes the task of creating a realistic and thorough numerical model more complicated in comparison to the modeling of non-magnetized discharges. The difficulties come from several directions. A general limitation in the choice of the model comes from the low operating pressures. In particular, it makes the approximations, needed for a fluid description of the magnetron plasma, not necessarily valid. Even a stronger limitation for the use of the continuum models is the anomalous diffusion across the magnetic lines [6]. This means that the diffusion and mobility coefficients given by the classical theory [6], when used in magnetron simulations, predict a situation where the electron movement across the magnetic field lines is extremely restricted and the discharge has almost no conductivity [7]. The effect is proportional to the ratio B/n, where B is the magnetic field and n is the background gas density. These obstacles are also present in the hybrid models [8], where the energetic electrons are treated as particles and the rest of the plasma as fluid. An attempt to circumvent this problem by obtaining the transport coefficients in crossed electric and magnetic fields solving the Boltzmann's equation has been proposed [9], [10]. The data acquired in that way, however, are parametric towards the reduced electric and the reduced magnetic field, which makes them of limited use for practical calculations.

According to the above discussion, a numerical model, designated for modeling of sputter magnetrons in a broad operational range, should be kinetic. However, the non one-dimensional and spatially inhomogeneous magnetic field in most of the magnetrons makes the simulations based on numerical solution of the Boltzmann's equation impractical. Thus, the only remaining available technique is the particle-in-cell-Monte Carlo collisions (PIC-MCC) [11]. Note that although PIC-MCC is a different technique than the solution of the Boltzmann's equation, it has been proven that a result obtained by PIC-MCC converges to the solution of the Boltzmann's equation in the limit of a small time-step [12].

The existing kinetic numerical simulations of sputter magnetrons can be divided in two major groups. The first group threats the plasma as consisting of electrons, gas ions and gas atoms (normally argon with homogeneous density). Self-consistent simulations (i.e., the electric field is calculated as a superposition of the applied external field and the field created by the charged particles) of that kind are, as an example, [13]-[15].

The second group deals with the transport of the sputtered atoms. These are usually some kind of direct Monte Carlo simulations (DMCS) [16]-[18]. In this case the main needed assumption is the spatial and energy distribution of the bombarding ionic flux, which is used as an input. The possible influence of the sputtered ions upon the plasma potential distribution is not taken into consideration. The same holds for the self- and the atom-impact sputtering. In both groups the question of possible gas heating, resulting from the collisions of the gas atoms with the rest of the plasma species, is not addressed. According to [19], however, this effect can be very

Manuscript received October 17, 2005; revised January 24, 2006.

I. Kolev is with Research Group PLASMANT, University of Antwerp, Universiteitsplein 1, Wilrijk 2610, (phone: +32 3 820-23-82; fax: +32 3 820-23-76; e-mail: ivan.kolev@ ua.ac.be).

A. Bogaerts is with Research Group PLASMANT, University of Antwerp, Universiteitsplein 1, Wilrijk 2610, (annemie.bagaerts@ ua.ac.be).

strong, depending on the operating conditions and the type of gas. Consequently, it should be included in magnetron simulations. So far, a complete model, incorporating self-consistently all plasma species and the gas heating in a sputter magnetron, has not been reported.

The purpose of this paper is to present a 2d3v, self-consistent PIC-MCC model of a dc planar sputter magnetron that includes both charged and energetic neutral plasma species, accounts for the gas heating, and incorporates an external electric circuit. The importance of the circuit will be discussed later. The model is used to investigate a typical sputter magnetron and main discharge characteristics are presented. This includes, among others, calculated potential distribution, density profiles of the main plasma species, distribution of the gas temperature, and sputtered flux.

II. Description of the Magnetron

The scheme of the planar magnetron used in the present simulation is shown in Fig. 1. It is a Von Ardenne PPS 50 magnetron (commercially available), used with plasma shield (the side wall on the scheme in Fig. 1). The axisymmetric magnetic field is created by two concentric magnets located under the powered electrode - the cathode. The magnetron is balanced, which means that the majority of the magnetic flux lines originate at and return to the cathode surface without crossing the anode.

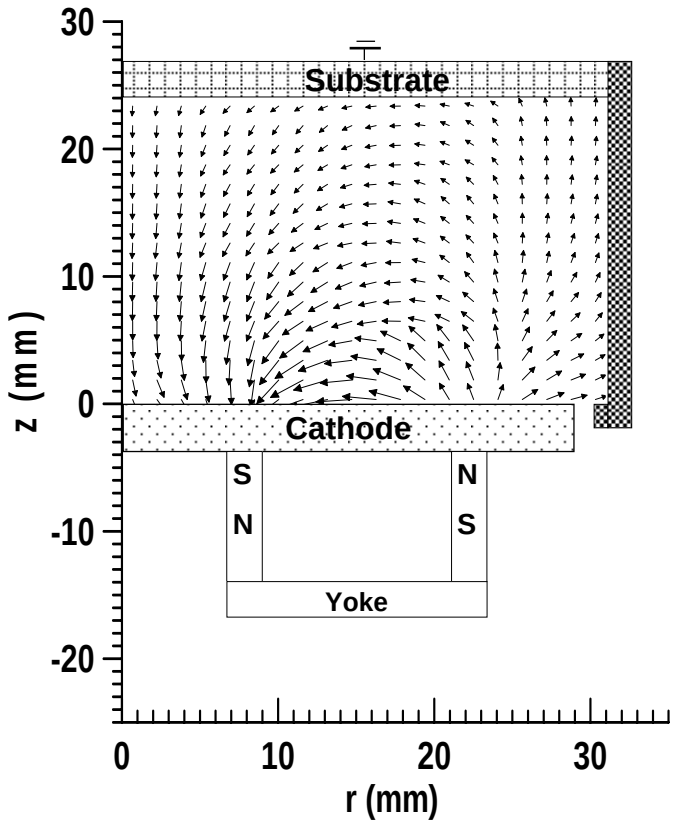

Fig. 1 Scheme of the magnetron.

All walls, except the cathode, are grounded and act as an anode. The smallest separation between the electrodes is equal to 2 mm and the distance between the cathode and the opposite anode plate, where the substrate is mounted, is 24 mm. The cathode is a copper disk with a thickness of 3 mm and a diameter of 58 mm. The discharge is maintained by a dc power supply, which can be run in a constant current or in a constant voltage mode. The magnetic field used in the simulation has been experimentally measured when the discharge has been not operational [20]. Experimental measurements of the discharge voltage as a function of the gas pressure and the magnetic field for the same system are reported in [21].

III. Description of the Model

A fully comprehensive model of a sputtering dc magnetron should include in a self-consistent manner the following: (i) plasma module, where the transport and the collisions of all plasma species of interest (both charged and neutral) are resolved; (ii) electric field solver, where the electric field inside the chamber is calculated; (iii) plasma-surface interaction module, where collisions of the plasma species with the cathode and substrate are treated; (iv) external circuit module, where the correct value of the cathode potential is calculated and the operating regimes of constant current or constant voltage are correctly realized; (v) gas heating module, where the gas temperature is calculated, based on the collisional events in the discharge. Setting these criteria, it has been implicitly assumed that the magnetic field inside the chamber equals that of the external magnets, i.e. the magnetic field generated by the electron motion does not perturb the external magnetic field. The way these modules are implemented in the present simulation is discussed next.

Owing to the axial symmetry of the magnetic field and to the cylindrical symmetry of the discharge vessel, the whole discharge is assumed cylindrically symmetrical. Such claim has been justified for a similar system in [13], where the authors, performing a fully 3d simulation, have established the absence of angular dependence of the discharge parameters. Thus, the present simulation is performed in cylindrical (r,z) coordinate space. However, all the three velocity components are taken into account. This is necessary, in order to satisfy the energy conservation and for proper description of the electron gyration.

The model is applied to an argon discharge. The species taken into consideration are electrons (e^-), argon ions (Ar^+), fast argon atoms (Ar^f), metastable argon atoms (Ar_m^*), copper atoms (Cu) and copper ions (Cu^+). The flow chart of the model is shown in Fig. 2. The program starts with initial density and velocity distributions of the e^- and Ar^+ superparticles. Each superparticle stands for a large number of real particles. This number is known as weight and in the present simulation it is chosen to be 10^6. Initially, only argon ions and electrons are assumed present with equal and homogeneous density of $10^{14}\,m^{-3}$. For both species a

Maxwellian velocity distribution is assumed with a temperature of 0.026 eV and 1 eV respectively.

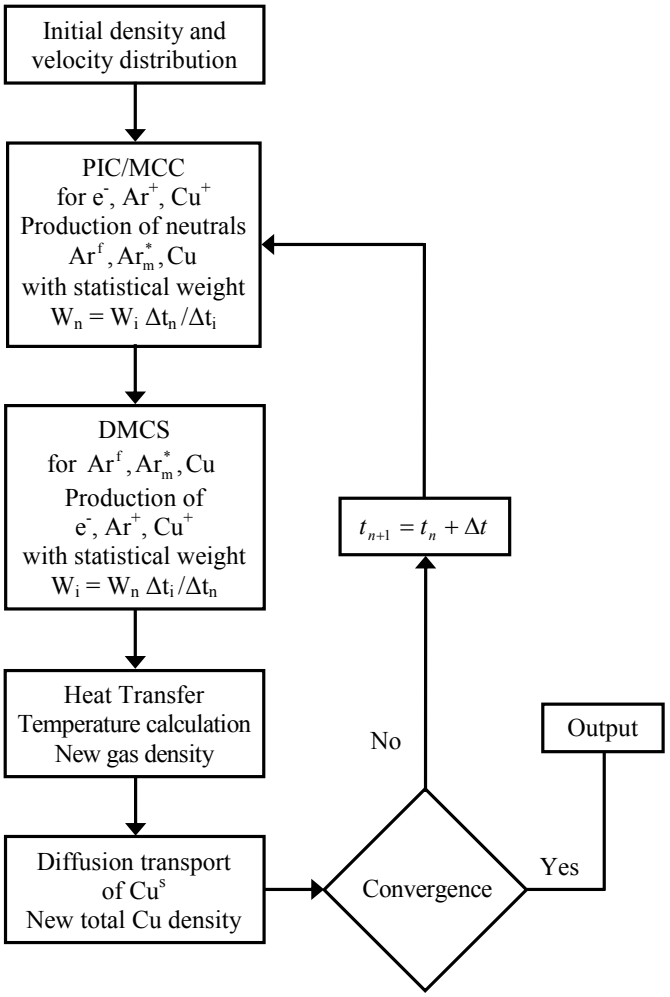

Fig. 2. Flowchart of the simulation procedure. The symbol Cu^s refers to the thermalized copper atoms.

They are traced in each time step, Δt, according to the PIC-MCC technique [11]. This means that their equations of motion

$$m\frac{d\boldsymbol{v}}{dt} = q\left(\boldsymbol{E} + \boldsymbol{v}\times\boldsymbol{B}\right),$$

where m is the mass, q is the charge, $\boldsymbol{v}(v_r, v_\theta, v_z)$ is the velocity, $\boldsymbol{E}(E_r, 0, E_z)$ is the electric and $\boldsymbol{B}(B_r, 0, B_z)$ is the magnetic field, is integrated numerically using the standard time-centered explicit integration scheme called "leap-frog" [22]. The rotation term is treated according to the algorithm suggested by Boris [23]. $\boldsymbol{E}$ is obtained as $\boldsymbol{E} = -gradV$, where V is the electric potential in the discharge, given by the Poisson's equation, which in (r,z) coordinates reads

$$\frac{1}{r}\frac{\partial}{\partial r}r\frac{\partial V(r,z)}{dr} + \frac{\partial}{\partial z}\frac{\partial V(r,z)}{\partial z} = -\frac{q}{\varepsilon_0}\left(n_i(r,z) - n_e(r,z)\right). \quad (1)$$

Here q is the elementary charge, ε_0 is the dielectric permittivity of free space and n_i and n_e are the ion (Ar^+, Cu^+) and electron densities. Equation (1) is solved using the cyclic reduction method [24]. By using the superposition principle, V can be presented as $V = V_P + U_0 V_L$, where V_P is the potential created by the space charge in the discharge, V_L is the dimensionless potential due to applied voltage with magnitude 1 in absence of space charge, and U_0 is the cathode voltage. Then V_P can be found as a solution of (1) with Dirichlet boundary condition, $V_P = 0$ at all boundary surfaces, except at $r = 0$. Since there is no linear charge at the origin, $r = 0$, the natural boundary condition there is

$$\left.\frac{\partial V_P}{\partial r}\right|_{r=0} = 0. \quad (2)$$

The potential, V_L, is a solution of Laplace equation

$$\Delta V_L(r,z) = 0 \quad (3)$$

with boundary conditions $V_L = 0$ at the grounded electrodes and $V_L = 1$ at the cathode. In the gap between the cathode and the anode at $z = 0$, V_L is assumed linearly decaying from 1 to 0 with the distance from the cathode edge. At $r = 0$ again (2) is imposed with V_L, instead of V_P. Equation (3) needs to be solved only once at the beginning of the simulation. Equations (1) and (3) are discretized using a standard five-point stencil and solved on a grid with $\Delta r = 0.32$ mm and $\Delta z = 0.08$ mm

In this simulation a simple circuit (Fig. 3), consisting of a constant voltage source and a ballast resistor in series with the discharge, is employed. The coupling between the circuit and the discharge is maintained by satisfying the charge conservation at the cathode

$$A\frac{d\sigma}{dt} = I_{ext}(t) + Q_{disch}, \quad (4)$$

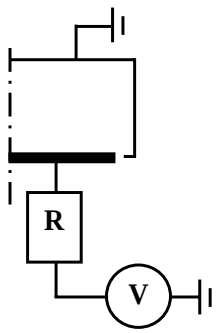

Fig. 3. Sheme of the external circuit.

where σ is the total surface charge at the cathode, I_{ext} is the external circuit current, A is the cathode surface and Q_{disch} is the net charge, deposited from the discharge on the cathode during a period dt, divided by the period.

The total surface charge can be determined independently of (4) applying the Gauss's theorem on a box surrounding the cathode. Then according to the Kirchhoff's voltage loop law, the cathode potential is equal to $U_0 = V_{ext} - R_{ext}I_{ext}$. The overall principles

of simultaneous circuit and discharge simulation are given in [22]. A detailed numerical procedure for the case of (*x,y*) Cartesian geometry for LC circuit is proposed in [25]. In the present model, a procedure for the circuit in Fig. 3 in (r,z) cylindrical geometry is developed based on the principles in [22] and [25].

At the middle of the time step, the probability of the k-th type of collision

$$P_k = 1 - \exp\left(N_{tar} \sigma_k \left(\varepsilon_i \right) \sqrt{2\varepsilon_i / m_i} \Delta t \right) \tag{5}$$

is examined and compared to a random number, uniformly distributed in [0,1]. Here σ_k is the corresponding cross-section. ε_i is the energy of the incident particle, m_i its mass, and N_{tar} is the density of the target species. The list of the considered collisions is given in Table I. The references for their cross sections or rate constants can be found in [26]-[43]. Coulomb collisions are also included. Their importance is in changing the momentum of the electrons and thus contributing to their mobility. Although Coulomb interactions are long-range collisions, it is possible to treat them as if being short-range. This is achieved by gathering of many small angle collisions in a single binary collision [44]. Inclusion of collisions, which are different from interactions between plasma species and the feeding gas, demands explicit knowledge of which exactly particles are located in a given grid cell at any time. In the code it is realized by performing sorting of the particles after each time step. This sorting also accelerates the calculations for reasons related to the processors' architecture. More details about this, as well as the sorting algorithm, are given in [45].

There are a few things that are worth to mention. First, when the elastic scattering of electrons from argon is treated, it should not be considered as being isotropic. The anisotropy of this process for the electron energies of interest is a well-established fact, both experimentally [46] and theoretically [47]. In magnetrons, where the conductivity is due to collisions (otherwise the electrons would never escape the magnetic trap and reach the anode), assuming isotropic scattering in models always leads to wrong results. A convenient analytical expression for the scattering angle, χ, in c.m. system as a function of the electron energy, ε_e is given in [48]

$$\chi = arccos\left(1 - \frac{2RN}{1 + 8E\left(1 - RN\right)} \right),$$

where $RN \in [0,1]$ is a uniformly distributed random number, $E = \varepsilon_e / E_0$, and E_0 is the atomic unit of energy ($E_0 = 27.21\,\text{eV}$). Second, the total integrated elastic cross section is needed and not the elastic momentum transfer cross-section. Third, the use of the null-collision technique [49] is not correct in the case of electron and ion collisions in magnetrons. The null-collision technique works well when particles exhibit swarm-like behavior, which is not the case in magnetrons. A very useful collision algorithm, allowing with a single random number to determine not only whether a collision takes place, but also what type of collision occurs, is given in [50].. Fourth, the geometry of the magnetic field and the low operating pressure allow to significant number of secondary electrons to return to the cathode and to be recaptured. The effect of this recapture upon the discharge characteristics is shown to be big and complex [15]. Consequently, any simulation of magnetrons is very sensitive towards the value of the reflection/absorption coefficient of the electrons at the cathode [15]. A self-consistent procedure to calculate this value, as a function of the electron energy, is given in [51].

Once the scattering angle is known, the new post-collision velocities as a function of χ are calculated according to [52].

Due to the big disparity in electron and ion mass the ions are moved only once per 20 electron time steps. This is done for speeding up the procedure. After every ion time step the number of the SP's in the system is checked and if increased above some predetermine limit it is reduced twice. The particles to be discarded are selected randomly and the weight of the remaining is doubled.

The stability criterion of the leap-frog algorithm limits the time step. For a Maxwellian plasma it reads [22]

$$\omega_{ch} \Delta t \le 1.62\,, \tag{6}$$

where ω_{ch} is the characteristic frequency in the simulated system. Here, ω_{ch} is the angular and not the linear frequency, because (6) is based on the harmonic oscillator model. Two frequencies should be checked in magnetrons. The electron plasma frequency,

$$\omega_{pe} = \sqrt{n_e q_e^{\,2} / \varepsilon_0 m_e}$$

and the electron gyro frequency,

$$\omega_{ge} = q_e B / m_e\,,$$

where m_e and q_e are the mass and the charge of the electron. Then, $\omega_{ch} = max\left\{ \omega_{pe}, \omega_{ge} \right\}$. In the present simulation B does not exceed 0.12 T, so $\omega_{ge} \le 2.12 \times 10^{10}$ rad/s. ω_{pe} depends on n_e, which is not known in advance and can vary largely during the simulation. Therefore, every 5000 time steps the maximum n_e is determined and Δt is adjusted to satisfy (6). Thus, Δt varies during the simulation between, approximately, 10^{-10} s and . 10^{-12} s.

Another very important restriction is the Courant criterion

$$v \Delta t / \Delta z \le 1\,, \tag{7}$$

where v is some mean characteristic velocity. Equation (7) guarantees that not too many SP's are jumping over field variations, which leads to numerical heating. In equilibrium plasmas v can be replaced by the electron thermal velocity. Magnetrons are nonequilibrium plasma devices. The discharge exists due to the presence of highly energetic nonequilibrium electrons emitted from the cathode. If Δt is fixed to obey (7) for their typical velocities, this will result in very long computational times. However, since these fast electrons are only a tiny fraction of the whole electron population, Δt is set to obey (6) only. The Courant criterion is fulfilled by checking the path, Δs, traveled by each electron in a time step. If $\Delta s > \Delta z$, the electron is returned to its initial position, and then moved twice with $0.5\Delta t$ in a manner preserving time centering. The procedure is iteratively repeated until Δs becomes smaller than Δz.

The movement of the fast neutrals is essentially inertial with change of the velocity only due to collisions. Collision probabilities are calculated again using (5). Fast gas atoms are traced in order to account for the heating of the gas and for their role in producing of sputtered atoms at the cathode. The metastable gas atoms contribute to the ionization of the sputtered atoms via Penning ionization. The sputtered atoms are created at the cathode by ion and fast atom bombardment. Each time an energetic ion or atom hits the target a random number is generated and compared with the sputtering yield, Y given by [53]

$$Y(\varepsilon_i) = 0.42\frac{\alpha Q K_s s_n(\varepsilon_i)}{U_s\left[1+0.35U_s s_e(\varepsilon_i)\right]}\left[1-\left(E_{th}/E\right)^{1/2}\right]^{2.8}$$

where ε_i is the energy of the incident particle, U_s is the sublimation energy of the cathode material [53], E_{th} is the threshold energy, and the other symbols are parameters related to the cathode material. This formula does not take into consideration the angular distribution of the incident flux. The sputtered atoms, generated in this way, are followed until they are thermalized. Afterwards, their further transport is considered to be diffusion-dominated and obtained by solving the diffusion equation. Thus, the total sputtered atom density is a sum of the densities of the fast sputtered atoms and the thermalized sputtered atoms.

The background gas is assumed to be initially at room temperature (300 K) with a constant density. During the simulation the energy transfer between plasma species and the gas is calculated and the temperature of the gas is periodically recalculated leading to a non-constant gas density. The effect of heating is dependent on the pressure and on the dimensions of the chamber. The gas temperature, T_g, is obtained by solving the heat conduction equation, which in cylindrical (r,z) coordinates reads

$$\frac{\partial^2 T_g}{\partial z^2}+\frac{1}{r}\frac{\partial}{\partial}\left(r\frac{\partial T_g}{\partial r}\right)=-\frac{P}{k}$$

where k is the thermal conductivity of the feeding gas and P is the transferred power density:

$$P=\frac{m_g W_n}{V_{cell}\Delta t_n}\left[\sum_k \frac{v_k'^2-v_k^2}{2}-\sum_k{}' \frac{v_k^2}{2}+\sum_k{}'' \frac{v_k'^2}{2}\right]$$

with v_k' being the post- and v_k pre- collision velocity of the gas atom, W_n is the neutral weight, m_g is the gas atom mass, Δt_n is the neutral time step, and V_{cell} is the volume of the computational grid cell. The first sum is the contribution from all collisions between the gas atoms from one side and the ions, fast and metastable gas atoms, and the sputtered atoms from the other side. Only collisions, where the post-collision energy of the gas atom is less than some threshold are counted. This threshold is chosen to be, $E_{th}=\left(9\times 3/2\right)k_b T_g$ [54]. The other collisions result in creating fast gas atoms, which are incorporated by the second sum. The third sum is the contribution of the thermalized fast gas atoms. Because the characteristic time steps of the electrons, ions, fast neutrals, and thermal conduction differ by as much as a factor of 10^6, some modifications are necessary to cope with this disparity. Not doing so would result in a huge amount of computational time. The procedure used here [54] is to advance the different sorts of particles with different time steps. The hierarchy being $\Delta t_e << \Delta t_i << \Delta t_n$ (e-electron, i-ion, and n-neutral). This difference in the time steps is accounted for by the weight, W of the produced energetic charge-exchange neutrals and sputtered atoms, i.e.,

$$W_n = W_s = W_i\frac{\Delta t_n}{\Delta t_i},$$

where s refers to the sputtered atoms. Electrons are subcycled inside the ion time step and have $W_e = W_i$. The simulation is run until convergence is reached (Fig. 2). The latter is assumed when the number of the simulated particles, the

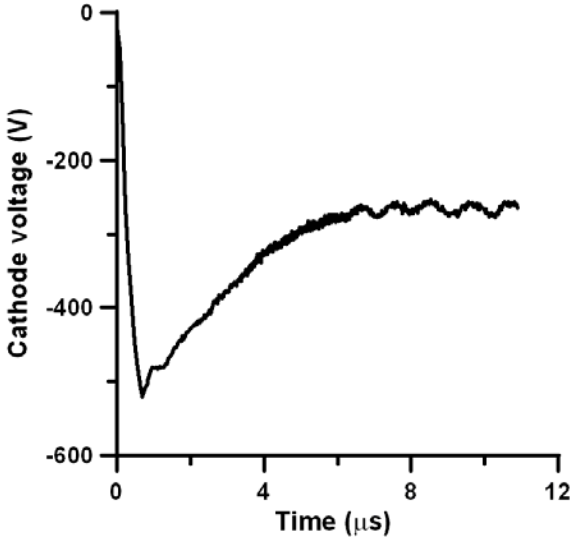

Fig. 4. Time evolution of the cathode potential Convergence is achieved after app. 10 μs.

TABLE I
INCLUDED REACTIONS

Processes		Cross section / rate	Reference
$e^- + Ar \rightarrow e^- + Ar$	elastic scattering	σ(e)	[26]
$e^- + Ar \rightarrow 2e^- + Ar$	electron-impact ionization	σ(e)	[27]
$e^- + Ar \rightarrow e^- + Ar_m^*$	electron-impact excitation	σ(e)	[28]
$e^- + Ar \rightarrow e^- + Ar^*$	electron-impact excitation	σ(e)	[26]
$e^- + Ar_m^* \rightarrow 2e^- + Ar^+$	electron-impact ionization	σ(e)	[29]
$e^- + Ar_m^* \rightarrow e^- + Ar^*$	electron-impact excitation	σ(e)	[30]
$e^- + Ar_m^* \rightarrow e^- + Ar_r^*$	electron quenching	$k_q = 2 \times 10^{-13}$ m^{3}s^{-1}	[31]
$e^- + Ar^+ \rightarrow Ar_m^* + h\nu$	electron-ion recombination	$k_{rec} = 10^{-17}$ m^{3}s^{-1}	[32]
$e^- + Cu \rightarrow e^- + Cu^+$	electron-impact ionization	σ(e)	[33]
$Ar^+ + Ar \rightarrow Ar^+ + Ar$	elastic scattering	σ(e)	[34]
$Ar^+ + Ar \rightarrow 2Ar^+ + e^-$	ion-impact ionization	σ(e)	[34]
$Ar^+(Ar^f) + Ar \rightarrow Ar^+(Ar^f) + Ar_m^*$	ion- (atom-) impact excitation	σ(e)	[35]
$Ar^+ + Cu \rightarrow Ar + Cu^+$	asymmetric charge transfer	σ(e)	[36]
$Ar_m^* + Ar_m^* \rightarrow Ar + Ar^+ + e^-$	metastable-metastable collision	$k_{mm} = 6.4 \times 10^{-19}$ m^{3}s^{-1}	[37], [38]
$Ar_m^* + Cu \rightarrow Ar + Cu^+ + e^-$	Penning ionization	σ(e)	[39]
$Ar_m^* + Ar \rightarrow Ar + Ar$	two-body collision	$k_{2b} = 2.3 \times 10^{-21}$ m^{3}s^{-1}	[40]
$Ar^f + Ar \rightarrow Ar^{(f)} + Ar^{(f)}$	elastic scattering	σ(e)	[41]
$Ar^f + Ar \rightarrow Ar + Ar^+$	atom-impact ionization	σ(e)	[42]
$Cu^{(+)} + Ar \rightarrow Cu^{(+)} + Ar$	elastic scattering	σ(e)	[43]

cathode voltage, the ionization rates of argon and copper and the maximum value of the electron density, all relax to steady state values. The typical convergence times are around 20 μs. As an example, the time evolution of the cathode voltage is shown in Fig. 4.

IV. RESULTS OF THE MODEL

The model is applied to the magnetron in Fig.1 with the following operating conditions: pressure p = 5 mtorr, feeding gas argon, cathode material copper, *Vext* = 850 V, *Rbal* = 1100 Ω, maximum magnetic field, B = 1200 G.

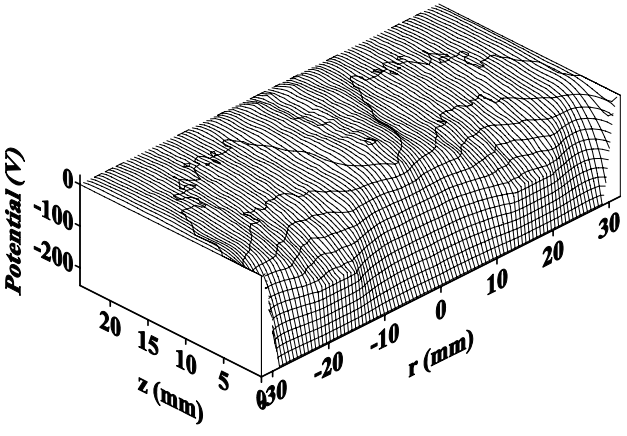

Fig. 5. Calculated potential.

In Fig. 5 the calculated distribution of potential, V, and in Fig. 6 the axial component of the electrical field, E_z, are shown. The potential is entirely negative above the racetrack with a minimum sheath thickness of approximately 0.9 mm at r = 18 mm, where the radial component of the magnetic field is maximal. The negative potential is connected to a region of a negative space charge, formed due to the very limited mobility of the electrons. In fact, their transport across the magnetic field lines is only possible due to collisions. The sheath exhibits strong radial dependence. Around the symmetry axis at r = 0, where the magnetic field is almost perpendicular to the cathode, it is much thicker and the space charge is positive. The electric field reaches very strong values in the sheath – up to 600 kV/m and has also a strong radial dependence. This is an illustration of the statement that making assumptions about the field strength and shape in planar magnetrons is unreliable.

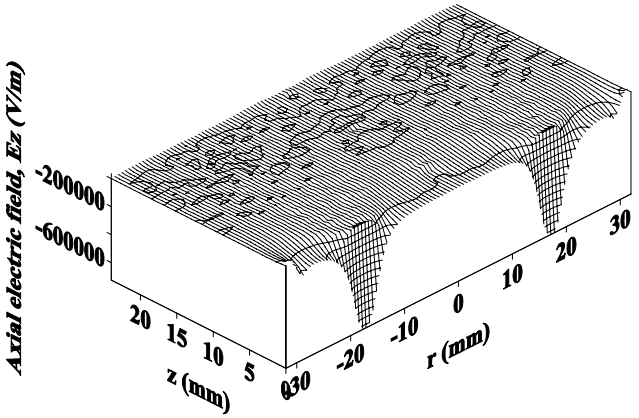

Fig. 6. Calculated axial electric field, E_z.

The potential distribution is in good agreement with the measurements in [55] and confirms the existence of a negative space charge in magnetrons at high magnetic field and low pressure, predicted numerically for cylindrical magnetrons in [56].

The electron density (Fig. 7) is very well localized in the region between the magnet poles and has a maximum value of 9 x 10^{17} m^{-3}.

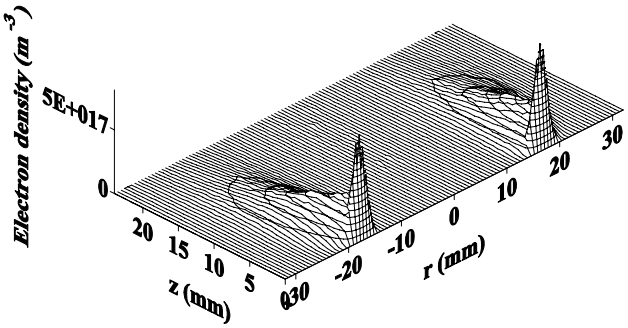

Fig. 7. Calculated electron density.

Except in the sheath, the Ar^+ density (not shown here) follows the electron density. The Cu^+ density (Fig. 8), is approximately two orders of magnitude lower than the Ar^+ density, thus the contribution of the Cu^+ ion to the charge density is marginal

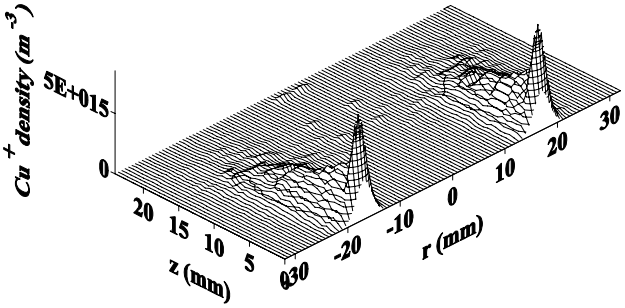

Fig. 8. Calculated copper ion (Cu^+) density.

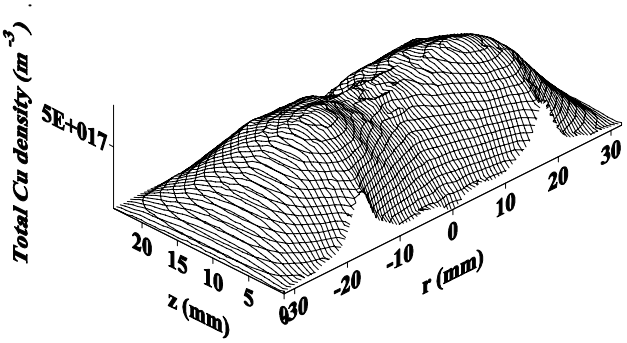

Fig. 9. Calculated total copper atom density.

The sputtered Cu atom density (Fig. 9) has a maximum of app. 10^{18} m^{-3} and is relatively homogeneously distributed. Due to the low pressure and the small discharge cell there is a significant fraction of Cu atoms with energies of a few eV, which reach the substrate. The main mechanism for production of sputtered atoms at the given operating conditions is the Ar^+ bombardment of the cathode. Self-sputtering is calculated to be negligible. The relative contribution to the sputtered flux is shown in Fig. 10.

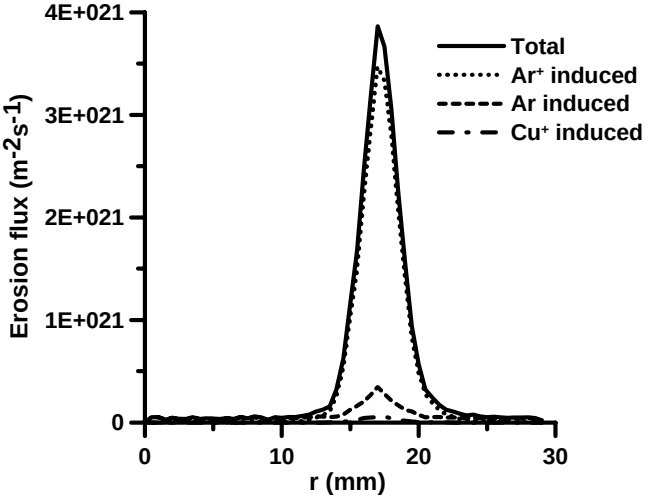

Fig. 10. Calculated erosion flux; solid line: total; dotted line: Ar^+ induced, dashed line Ar^f induced, dash – dotted line Cu^+ induced.

Gas heating is moderate at a pressure of 5 mtorr. The gas temperature rises only to 320 K. The main mechanism is the atom-atom interactions. The energy loss in Ar^+ - Ar collisions contributes indirectly to gas heating, *i.e.*, in first instance fast Ar atoms are created and later on they thermalize by colliding with the cold Ar atoms.

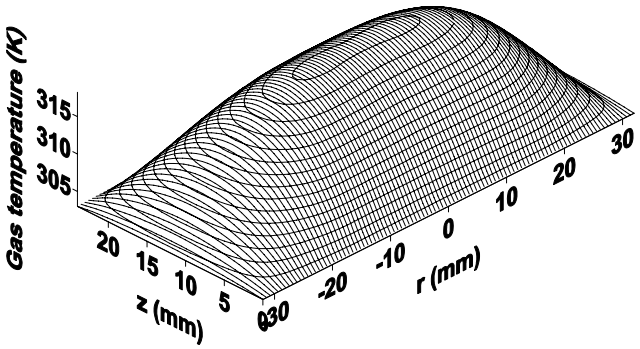

Fig. 11. Calculated gas temperature at p = 5 mtorr.

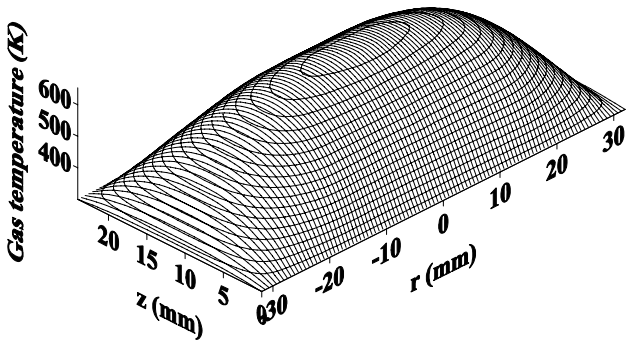

Fig. 12. Calculated gas temperature at p = 50 mtorr.

The overall calculated temperature distribution is shown in Fig. 11. To illustrate the relation between gas heating and gas pressure a simulation is carried for p = 50 mtorr, with the

other operating conditions identical. As it can be seen in Fig. 12, in his case gas heating can not be neglected, because the gas temperature rises to about 600 K.

To verify the model the calculated erosion profile is compared to the experimentally measured one [20] at approximately the same operating conditions after 4 hours of sputtering. The results are shown in Fig. 13. A very reasonable agreement can be seen. Both maxima coincide perfectly and the shape of the crater is almost identical. The experimental magnetron has been operated in a constant current regime of 0.4 A. The calculated discharge current is 0.412 A. To obtain the latter value the simulation has been run for 5 μs after convergence has been reached. Sampling has been taken every 0.2 μs and the results averaged.

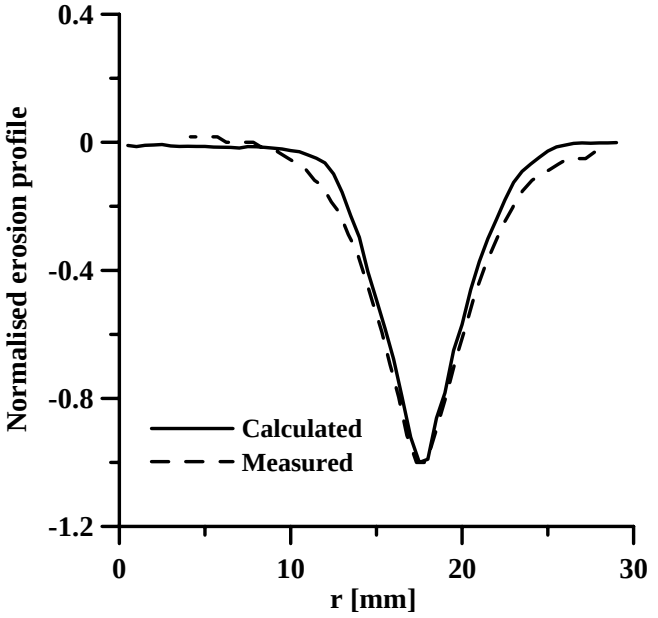

Fig. 13. Calculated (solid line) and measured (dashed line) normalized erosion profile.

V. Conclusion

A 2d3v, self-consistent numerical model based on PIC-MCC technique has been developed to simulate planar dc sputter magnetrons. The model deals with the charged particles in the discharge, as well as, with the sputtered neutrals and energetic gas atoms. All mechanisms for ionization of the sputtered atoms are included. The effect of the gas heating is taken into account. An external circuit is added in a self-consistent manner to set the simulation into the desired part of the volt-ampere curve of the magnetron. By choosing the parameters of the circuit, regimes of constant voltage and constant current can be simulated. The model produces all important characteristics of the discharge, such as: the density profiles of all species into consideration, the electric potential and field distribution, the particle and energy fluxes towards the electrodes, the erosion profile, the gas temperature distribution, and the energy distribution functions.

The model has been applied to Von Ardenne PPS 50 magnetron, operated in Argon. The validity of the model is proven by comparing the calculated normalized erosion profile and discharge current with the experimentally obtained ones. The results show the presence of a negative space charge region at low pressure. Gas heating can be disregarded at p = 5 mtorr and applied power, P < 100 W. With increase of the pressure, however, it should be included in models. The main sputtering source is the Ar^+ ions.

The model is not limited to Ar only or to some specific operating conditions. It needs to be modified only for the case of non axisymmetric magnetic field. The presence of an external circuit makes it easy to adapt the model to cover rf or pulsed operating regimes

.

Acknowledgment

I. Kolev would like to thank Prof. Renaat Gijbels for numerous discussions and useful advises.

References

[1] R. K. Waits, "*Planar magnetron sputtering*," *J. Vac. Sci. Technol.*, vol. 15, pp. 179-187, March 1978.

[2] J. A. Thornton, "*Magnetron sputtering: basic physics and application to cylindrical magnetrons*," *J. Vac. Sci. Technol.*, vol. 15, pp. 171-177, March 1978.

[3] J. A. Thornton and A. S. Penfold, "*Cylindrical magnetron sputtering*," in *Thin Film Processes*, J. L. Vossen and W. Kern, eds. New York: Academic, 1978, p. 75.

[4] S. M. Rossnagel, "*Glow Dischrge Plasmas and Sources for Etching and Depoeition: Magnetrons*," in *Thin Film Processes II*, J. L. Vossen and W. Kern, Eds. Boston: Academic Press, 1991, pp. 46-62.

[5] J. A. Thornton, "*High rate sputtering techniques* ," *Thin Solid Films,* vol. 80, no. 1-3, pp. 1-11, June 1980.

[6] F. P. Chen, *Introduction to Plasma Physics and Controlled Fusion.* New York: Plenum Press, 1984, ch. 5.5

[7] I. Kolev and A. Bogaerts," Numerical Models of the Planar Magnetron Glow Discharges," *Contrib. Plasma Phys*., vol. 7-8, pp. 582-588, Nov. 2004.

[8] E. Shidiji, H. Ohtake, N. Nakano, and T. Makabe, "," *Jpn. J. Appl. Phys., Part 1*, vol. 38, pp. 2131-21, 1999.

[9] K. Ness and T. Makabe, "Electron transport in argon in crossed electric and magnetic fields," *Phys. Rev. E*, vol. 62, pp. 4083-4090, Sep. 2000.

[10] R. D. White, R. E. Robson, K. F. Ness and T. Makabe, "Electron transport coefficients in O_2 magnetron discharges," *J. Phys. D: Appl. Phys*.,vol. 38, pp. 997-1005, Apr. 2005.

[11] C K Birdsall, "Particle-in-cell charged-particle simulations, plus Monte Carlo collisions with neutral atoms, PIC-MCC," *IEEE Trans. Plasma Sci*., vol. 19, no. 2, 65-85, Apr. 1991.

[12] H. Babovsky and R. Illner, "A convergence proof for Nanbu's simulation method for the full Boltzmann Equation," *SIAM J. Numer. Anal.*, vol. 26, no. 1, pp. 45-65**,** Feb. 1989.

[13] S. Kondo and K. Nanbu, "A self-consistent numerical analysis of a planar dc magnetron discharge by the particle-in-cell/Monte Carlo method," *J. Phys. D: Appl. Phys*., vol. 32, pp. 1142-1152, May 1999.

[14] N. F. Cramer, "*Analysis* of a one-dimensional, steady-state magnetron discharge*," J. Phys. D: Appl. Phys.*, vol. 30, pp. 2573-2584, 1997.

[15] I. Kolev, A. Bogaerts, and R. Gijbels, "Influence of electron recapture by the cathode upon the discharge characteristics in DC planar magnetrons," *Phys. Rev. E*, vol. 72, 056402, Nov. 2005.

[16] K. Macak, P. Macak, and U. Helmersson, "Monte Carlo simulations of the transport of sputtered particles," *Comp. Phys. Commun.*, vol. 120, no. 2 - 3, pp. 238-254, Aug. 1999.

[17] Y. Kusumoto and K. Iwata, "Numerical study of the characteristics of erosion in magnetron sputtering," *Vacuum*, vol. 74, no. 3 – 4, pp. 359-365, June 2004.

[18] V. Serikov and K. Nanbu, "Monte Carlo numerical analysys of target erosion and film growth in a three-dimensional sputtering chamber," *J. Vac. Sci. Technol. A*, vol. 14, no. 6, pp. 3108-3123, Nov/Dec 1996.
[19] S. M. Rossnagel, "Gas density reduction effects in magnetrons," *J. Vac. Sci. Technol. A*, vol. 6, no. 1, pp. 19-24, Jan/Feb 1988.
[20] G. Buyle, University of Gent, Gent, Belgium, private communications, May 2004.
[21] D. Depla, G. Buyle, J. Haemers, and R. De Gryse, "Discharge voltage measurements during magnetron sputtering," *Surf. Coat. Technol.*, to be published.
[22] C. K. Birdsall and A. B. Langdon, *Plasma physics via computer simulations*. Bristol: IOP publishing, 1991.
[23] J. Boris, "Relativistic Plasma Simulation - Optimization of a Hybrid Code," in *Proc. 4rth Conf. Num. Simul. of Plasmas,* Washington DC, 1970, pp. 3-67.
[24] P. N. Swartztrauber, "A direct method for the discrete solution of separable elliptic equations," *SIAM J. Numer. Anal*., vol. 11, no. 6, pp. 1136-1150, Dec. 1974.
[25] V. Vahedi and G. DiPeso, "Simultaneous Potential and Circuit Solution for Two-Dimensional Bounded Plasma Simulation Codes," *J. Comput. Phys*., vol. 131, pp. 149-163, Feb. 1996.
[26] M. Hayashi, IPPJ - AM Research Rep. 19 *(unpublished)*. Available: ftp://jila.colorado.edu/collision_data/electronneutral/hayashi.txt.
[27] A. V. Phelps and Z. Lj. Petrovic, "Cold-cathode discharges and breakdown in argon: surface and gas phase production of secondary electrons," *Plasma Sources Sci. Technol*., vol. 8, no. 3, pp. R21-R45, Aug. 1999.
[28] N. J. Mason and W. R. Newell, "Total cross sections for metastable excitation in the rare gases," *J. Phys. B,* vol. 20, no.6, pp. 1357-1379, March 1987.
[29] H. A. Hyman, "Electron-impact ionization cross sections for excited states of the rare gases (Ne, Ar, Kr, Xe), cadmium, and mercury," *Phys. Rev. A*, vol. 20, no. 3, pp. 855-859, Sep. 1979.
[30] H. A. Hyman, "Electron-impact excitation of metastable argon and krypton," *Phys. Rev. A*, vol. 18, no. 2, pp. 441-446, Aug. 1978.
[31] D. P. Lymberopoulos and D. J. Economou, "Fluid simulations of glow discharges: Effect of metastable atoms in argon," *J. Appl. Phys.*, vol. 73, no. 8, pp. 3668-3679, Apr. 1993.
[32] M. A. Biondi, "Studies of the Mechanism of Electron-Ion Recombination. I", *Phys. Rev.*, vol. 129, no. 3, 1181-1188 Feb. 1963.
[33] L. Vriens, "Calculation of absolute ionisation cross sections of He, He^*, He^+, Ne, Ne^*, Ne^+, Ar, Ar^*, Hg and Hg^*," *Phys. Lett.*, vol. 8, pp. 260-261, Feb. 1964.
[34] A. V. Pheplps, "The application of scattering cross sections to ion flux models in discharge sheaths," *J. Appl. Phys*., vol. 76, no. 2, pp. 747-753, July 1994
[35] A. V. Pheplps and B. M. Jelenkovic, "Excitation and breakdown of Ar at very high ratios of electric field to gas density," *Phys. Rev. A*, vol. 38, no.6 , pp. 2975-2990, Sep. 1988.
[36] A. Bogaerts and R. Gijbels, "Role of sputtered Cu atoms and ions in a direct current glow discharge: Combined fluid and Monte Carlo model," *J. Appl. Phys.*, vol. 79, no. 3, pp. 1279-1286, Feb. 1996.
[37] C. M. Ferreira and A. Ricard, "Modelling of the low-pressure argon positive column," *J. Appl. Phys*., vol. 54, no. 5, pp. 2261-2271, May 1983.
[38] C. M. Ferreira, J. Loureiro and A. Ricard, "Populations in the metastable and the resonance levels of argon and stepwise ionization effects in a low-pressure argon positive column," *J. Appl. Phys*., vol. 57, no. 1, pp. 82-90, Jan. 1985.
[39] L. A. Riseberg, W. F. Parks, and L. D. Schearer, "Penning Ionization of Zn and Cd by Noble-Gas Metastable Atoms," *Phys. Rev. A*, vol. 8, no. 4 , pp. 1962-1968, Oct. 1973.
[40] K. Tachibana, " Excitation of the $1s_5$,$1s_4$, $1s_3$, and $1s_2$ levels of argon by low-energy electrons," *Phys. Rev. A*, vol. 34, no. 2, pp. 1007-1015, Aug. 1986.
[41] A. V. Phelps, C. H. Greene, and J. P. Burke, Jr., "Collision cross sections for argon atoms with argon atoms for energies from 0.01 eV to 10 keV," *J. Phys. B*, vol. 33, no. 16, pp. 2965-2983, Aug. 2000.
[42] A. V. Phelps, "Cross sections and swarm coefficients for nitrogen ions and neutrals in N_2 and Argon ions and neutrals in Ar for energies from 0.1 eV to 10 keV," *J. Phys. Chem. Ref. Data*, vol. 20, no. 3, pp. 557-573, 1991.
[43] R. S. Robinson, "Energetic binary collisions in rare gas plasmas," *J. Vac. Sci. Technol.* Vol. 16, no. 2, 185-188, March 1979.
[44] K. Nanbu and S. Yonemura, "Weighted Particles in Coulomb Collision Simulations Based on the Theory of a Cumulative Scattering Angle," *J. Comput. Phys*., vol. 145, no. 2, pp. 639-654, Sep.1998.
[45] K. Bowers, "Accelerating a Particle-in-Cell Simulation Using a Hybrid Counting Sort ," *J. Comput. Phys.*, vol. 173, no. 2, pp. 393-411, Nov. 2001.
[46] D. Cvejanovic and A. Ceowe, "Differential cross sections for elastic scattering of electrons from argon and krypton as a continuous function of energy," *J. Phys. B: At. Mol. Opt. Phys.*, vol. 30, no. 12, pp. 2873-2887, June 1997.
[47] W. C. Fon, K. A. Berrington, P. C. Burke, and A. Hibbert, "The elastic scattering of electrons from inert gases: III. Argon," *J. Phys. B: At. Mol. Phys.*, vol. 16, no. 2, pp. 307-321, Jan. 1983.
[48] A. Okhrimovskyy, A. Bogaerts, and R. Gijbels, "Electron anisotropic scattering in gases: A formula for Monte Carlo simulations," *Phys. Rev. E*, vol. 65, 037402, Feb. 2002.
[49] V. Vahedi and M. Surendra, "A Monte Carlo collision model for the particle-in-cell method: applications to argon and oxygen discharges," *Comp. Phys. Commun.*, vol. 87, no. 1-2, pp. 179-198, May 1995.
[50] K. Nanbu, "Simple Method to Determine Collisional Event in Monte Carlo Simulation of Electron-Molecule Collision," *Jpn. J. Appl. Phys. Part 1*, vol. 33,no. 8, pp. 4752-4753, Aug. 1994.
[51] M. A. Furman and M. T. F. Pivi, "Probabilistic model for the simulation of secondary electron emission," *Phys. Rev. ST Accel. Beams*, vol. 5, no. 12, 124404, Dec. 2002.
[52] W. G. Vincenti and C. H. Kruger, Jr., *Introduction to Physical Gas Dynamics*. Huntington: Robert E. Kruger Publishing Company, 1977, pp.352-358.
[53] N. Matsunami et al., "Energy dependence of the ion-induced sputtering yields of monatomic solids," Atom. Data Nucl. Data Tables, vol. 31, no, 1, pp. 1-80, July 1984.
[54] V. Serikov and K. Nanbu, "The analysis of background gas heating in direct current sputtering discharges via particle simulation," J. Appl. Phys., vol. 82, no. 12, pp. 5948-5957, Dec. 1997.
[55] J. W. Bradley, S. Thompson and Y. Aranda Gonzalvo, "Measurement of the plasma potential in a magnetron discharge and the prediction of the electron drift speeds," Plasma Sources Sci. Technol. Vol. 10, no. 3, pp. 490-502, Aug. 2001.
[56] T. A. van der Straaten, N. F. Cramer, I. S. Falconer, and B. W. James, "The cylindrical DC magnetron discharge: II. The negative space charge mode," J. Phys. D: Appl. Phys., vol. 31, no. 2, pp. 191-207, Jan. 1998.

Ivan Kolev received B. Sc. degree in engineering physics and M. Sc. degree in semiconductor physics from the University of Sofia, Sofia, Bulgaria in 1991 and 1998, respectively.

From 2000 he is a Ph. D. student at the University of Antwerp, Wilrijk, Belgium. His research is devoted to numerical modeling of magnetrons. Currently, he is preparing his defence.

Annemie Bogaerts received M. Sc. degree in chemistry and Ph. D. degree in science from the University of Antwerp, Wilrijk, Belgium in 1993 and 1996, respectively.

She became a professor of physical chemistry at the University of Antwerp in 2003 and is the head of the research group PLASMANT, at the University of Antwerp. Her current research interests include numerical simulations of different kind of gas discharges and plasma-solid interaction (e.g., for the purpose of thin film deposition and etching) as well as the modeling of laser-solid interaction (laser ablation).